Electronic Supplementary Material (ESI) for RSC Advances.

Supplementary Information

Modifying microstructure of algae-based active carbon and modelling supercapacitors using artificial neural network

Jiashuai Wang [a], *Zhe Li* [a, c], *Shaocun Yan* [a, c], *Xue Yu* [a], *Yanqing Ma* [a, b *], *Lei Ma* [a*]

[a] Tianjin International Center for Nanoparticles and Nanosystems, Tianjin University, 300072, P.R. China

[b] State Laboratory of Precision Measuring Technology and Instruments, Tianjin University, 300072, P.R. China

[c] School of Chemistry and Chemical Engineering, Shihezi University, 832003, P.R. China

E-mail: mayanqing@tju.edu.cn; lei.ma@tju.edu.cn.

Mechanism of KOH activation

It is noteworthy that KOH was used as the activating agent to construct micropores and control the mesopores size distributions. During the KOH activation process, the reactions between KOH and carbon materials starts with solid-solid reactions. Then proceeds via solid-liquid reactions at about 570 ^{o}C that occur by the following redox reaction (Equation (S1)). [1]

$$2C + 6KOH \rightarrow 2K_2CO_3 + 2K + 3H_2 \quad \text{(S1)}$$

$$K_2CO_3 \rightarrow K_2O + CO_2 \quad \text{(S2)}$$

$$C + K_2O \rightarrow 2K + CO \quad \text{(S3)}$$

Moreover, if the activation temperature achieves over than 600 ^{o}C, the as-formed K_2CO_3 (Eqs. (S1)) would transform into CO_2 and K_2O (Eqs. (S2)), and the K_2O can be further reacted with carbon to form metallic K (Eqs. (S3)).[2] Metallic K (Equation (S1) and (S3)) can diffuse into the carbon framework and expand the lattice leading to the increase of pore volume. Furthermore, the escape of H_2, CO_2, CO and H_2O gas from the biomass carbon can also transform some micropores into mesopores by opening up the closed pores.[3] After removing the intercalated metallic potassium and potassium-containing compounds by the hydrochloric acid washing, the expanded carbon lattices cannot be restored, therefore reasonably generating pores.

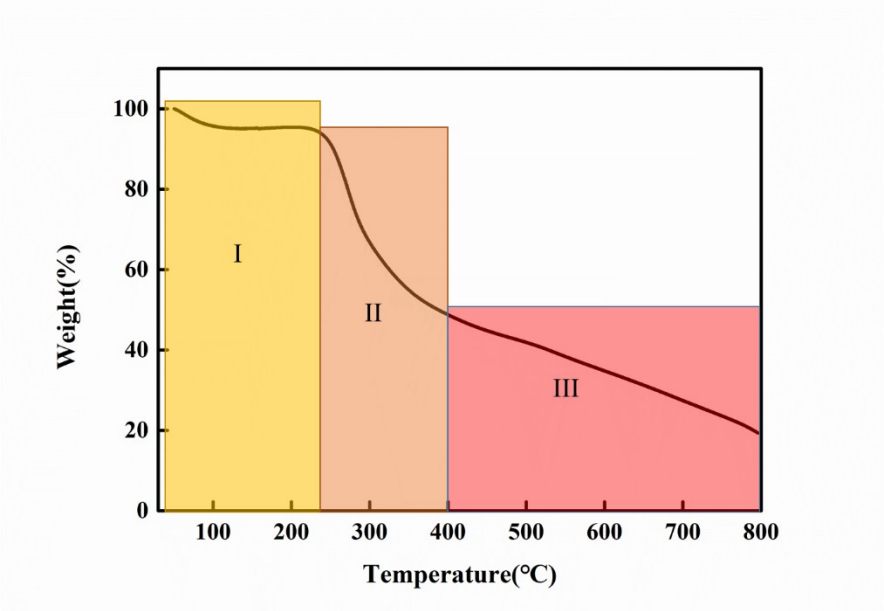

Fig. S1 TGA of dried NF algae under N_2 flow.

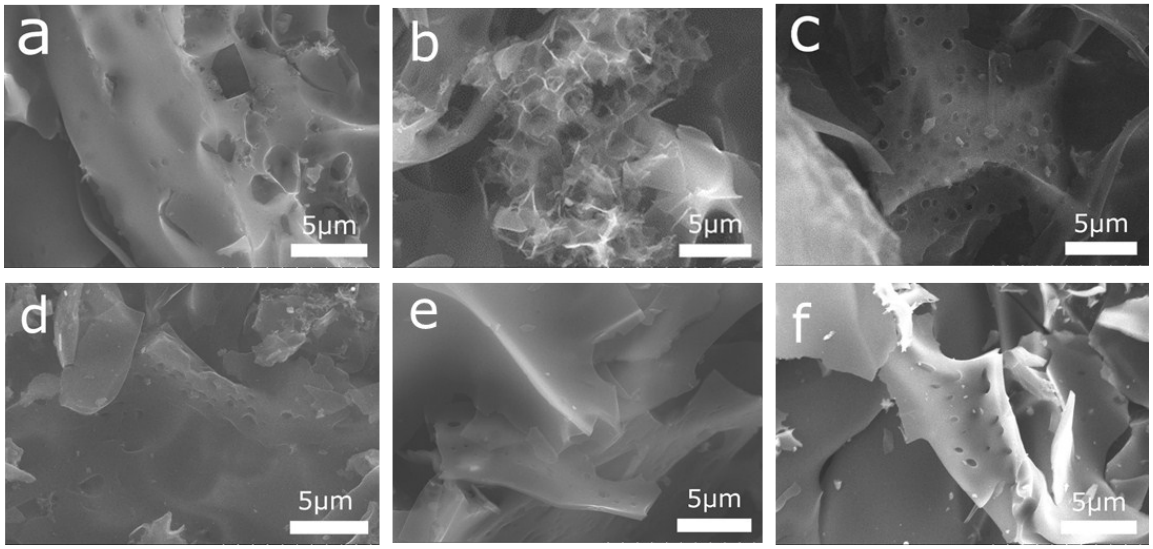

Fig. S2 SEM images for NFAC-c-600-3 (a), NFAC-c (b), NFAC-c-800-3 (c), NFAC-c-900-3 (d), NFAC-c-2 (e), NFAC-c-4.

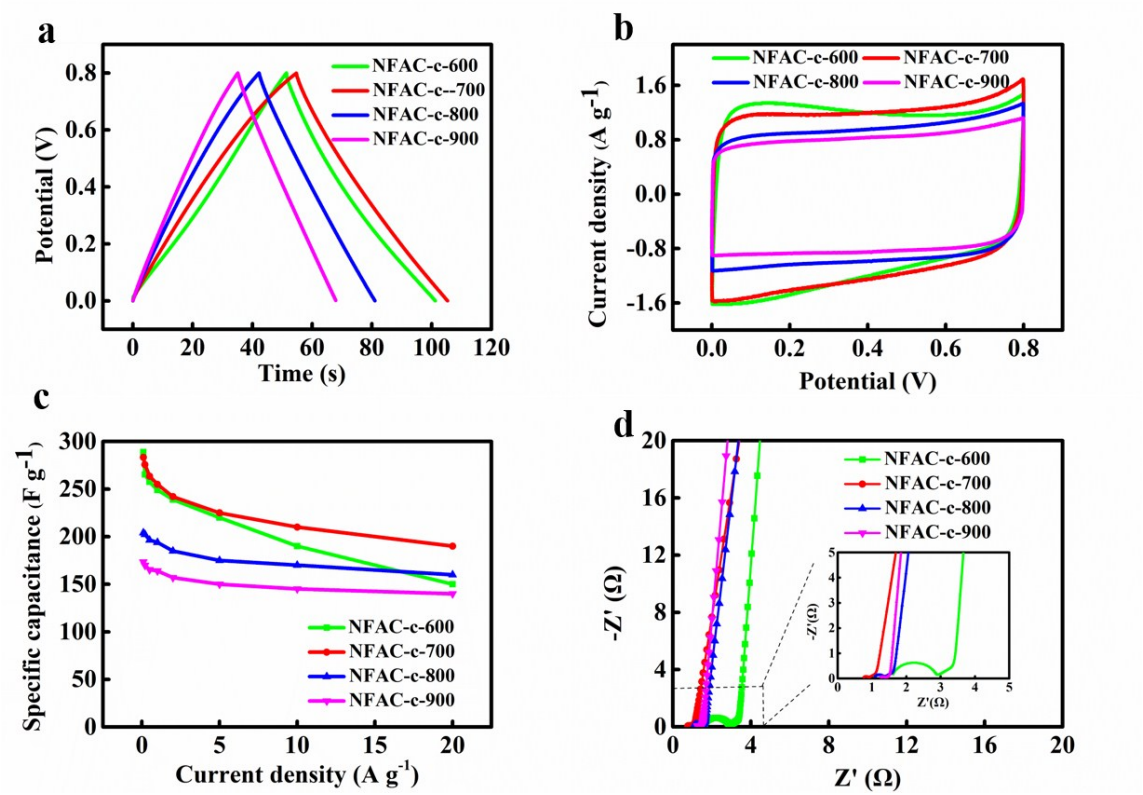

Fig. S3. Electrochemical behavior evaluation of NFAC-c-x (x present the activation temperature) in a two-electrode system: (a) CV curves at a scan rate of 20 mv s^{-1}; (b) GCD profiles at a current density of 1A g^{-1}; (c) Specific capacitance at various current density; (d) Nyquist plots.

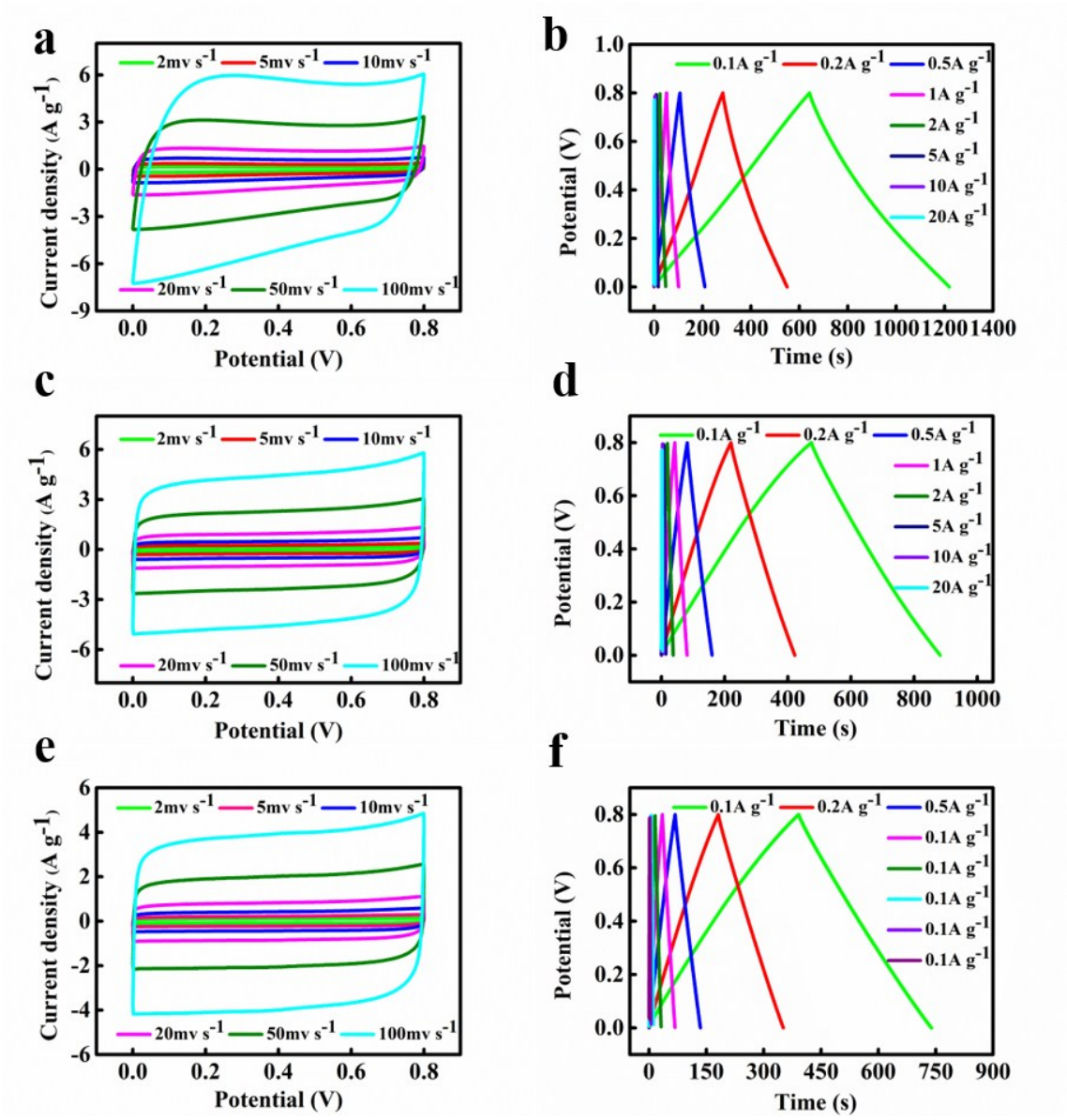

Fig. S4. CV and GCD curves of NFAC-c-600 (a, b); NFAC-c-800 (c, d), and NFAC-c-900 (e, f) in a two-electrode system.

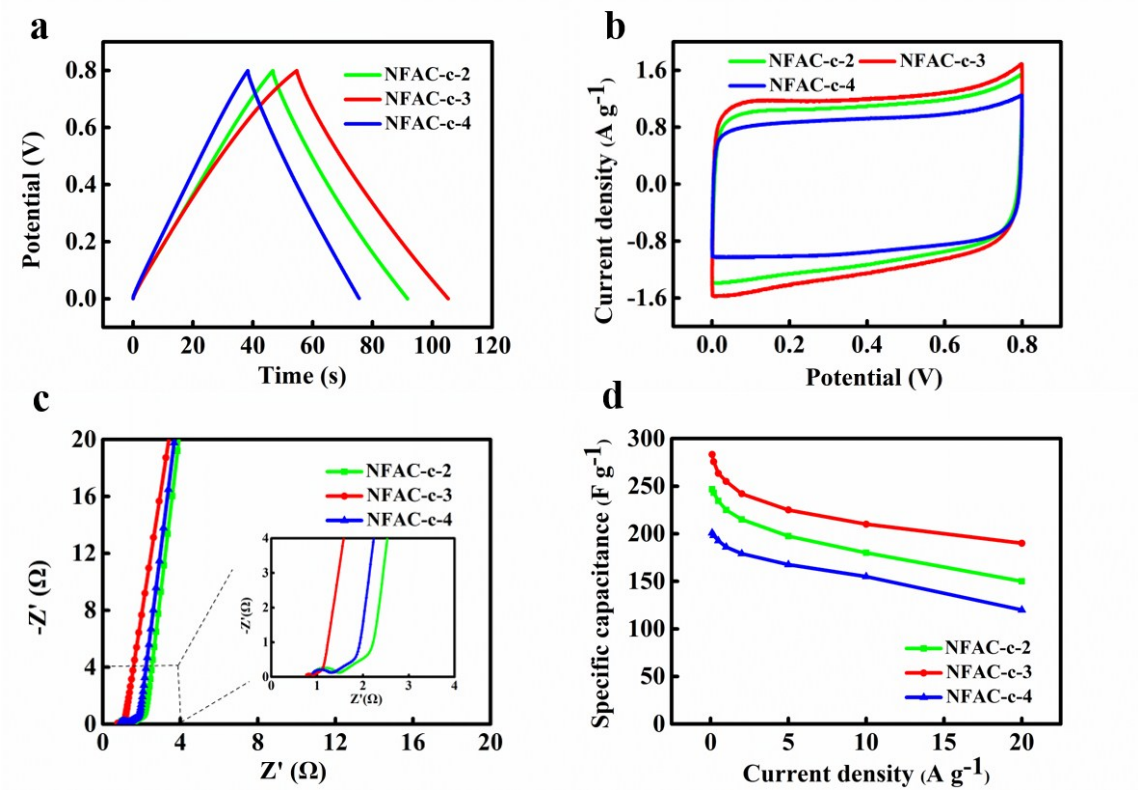

Fig. S5. Electrochemical behavior evaluation of NFAC-c-x (x represents the mass ratio of KOH/Carbon) electrodes in a two-electrode system: (a) CV curves at a scan rate of 20 mV s^{-1}. (b) GCD curves at a current density of 1.0 A g^{-1}. (c) Nyquist plots. (d) Specific capacitances as a function of charge/discharge current density.

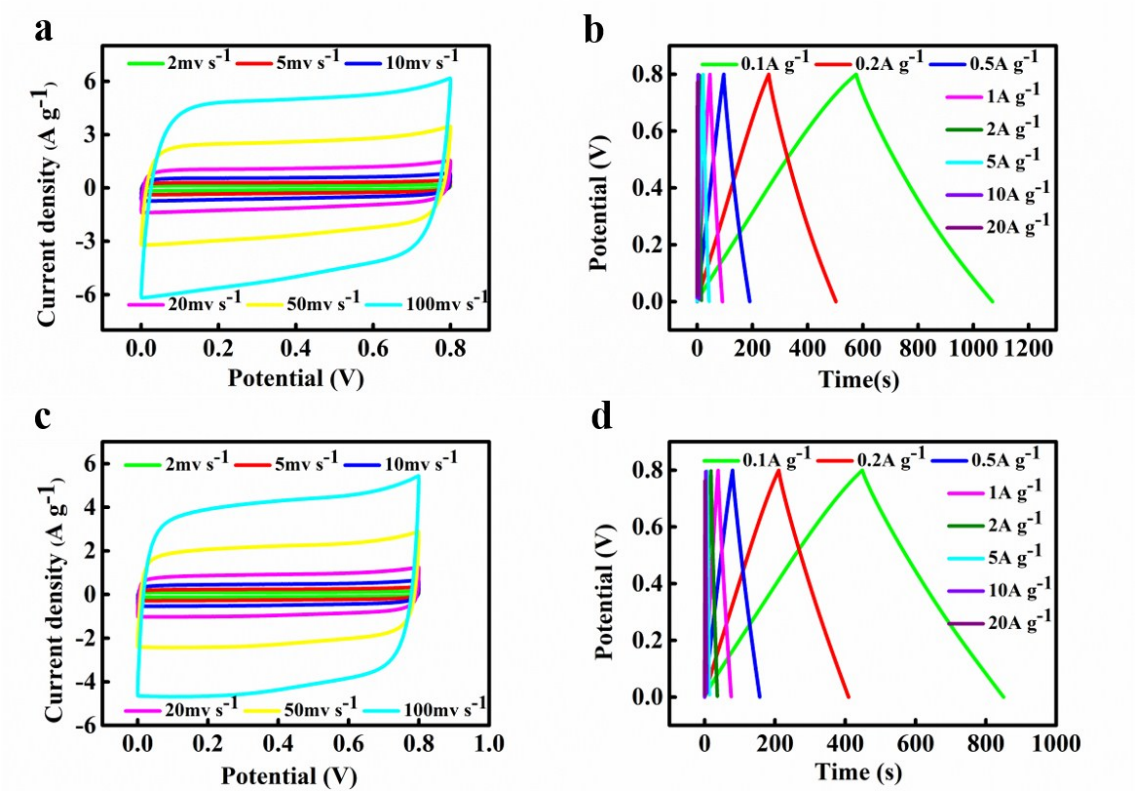

Fig.S6. CV and GCD curves of NFAC-c-2 (a, b); NFAC-c-4 (c, d).

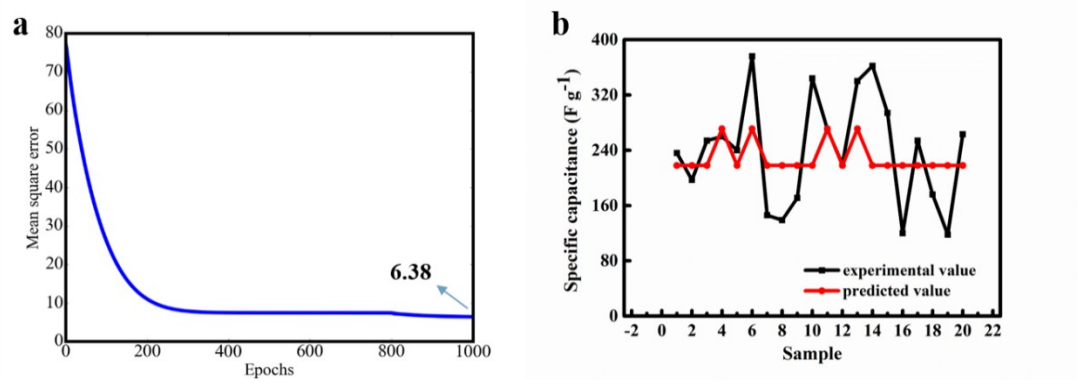

Fig.S7. The prediction effect of ANN model controlled by two inputs ($r_{L/D}$, CL (%)): (a) Mean square error as epochs. (b) Comparison of experimental and predicted value of test set for specific capacitance.

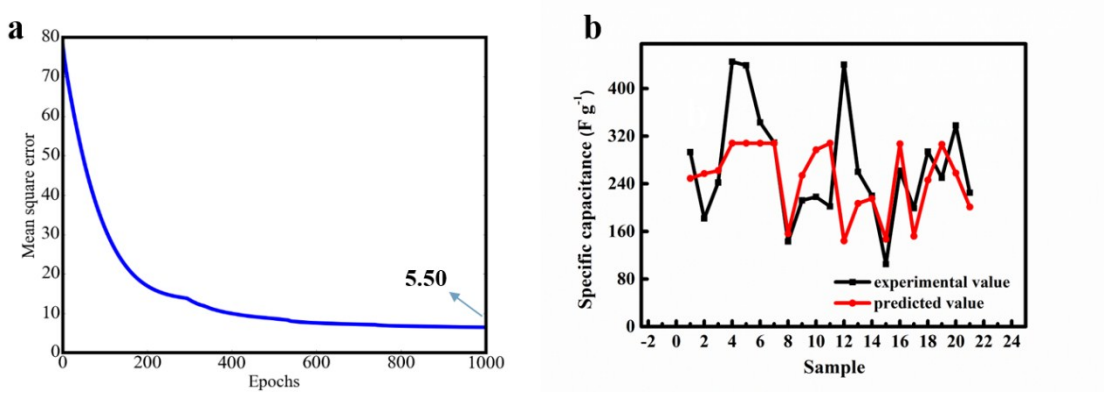

Fig. S8. The prediction effect of ANN model controlled by eight inputs (S_{BET}, D_{ave}, V_{tot}, V_{mic}, V_{mes}, I_D/I_G, R_s, N (%)): (a) Mean square error as epochs. (b) Comparison of experimental and predicted value of test set for specific capacitance.

Table S1 Diagram of interconnected weights of neutrons in input, hidden and output layer.

	H1	H2	H3	H4	H5	H6	H7	H8	H9	H10
I1	2.4	-5.1	55.0	-3.0	-4.7	-44.8	5.4	3.6	-3.9	-4.5
I2	3.2	-3.5	21.4	-3.8	-3.6	-14.0	4.6	2.5	-2.1	-3.7
O	25.4	-24.6	24.7	-24.8	-24.9	-24.6	25.0	24.7	-25.0	-24.1

I1: input layer1- $r_{L/D}$; I2: Input layer2 - CL (%); O: output layer.

Table S2 Diagram of interconnected weights of neutrons in input, hidden and output layer.

	H 1	H2	H3	H4	H5	H6	H7	H8	H9	H10
I 1	25.5	-2.7	-6.3	-17.8	2.9	-1.9	-2.5	-17.9	-21.1	8.8
I 2	4.9	-4.2	-4.2	4.9	6.8	-2.2	-0.6	-0.7	-6.8	-2.0
I 3	0.4	-2.5	-41.7	0.8	0.12	-2.3	-1.3	-20.6	-0.1	-23.9
I 4	15.8	-1.7	-18.9	12.9	5.06	-1.9	-1.4	-16.3	13.0	-17.0
I 5	-19.3	-2.2	12.9	-23.2	-2.3	-1.4	-2.7	7.0	9.8	21.8
I 6	-2.6	-0.5	7.4	3.1	0.7	-1.3	-2.7	-8.1	-8.4	25.7
I 7	72.7	-4.4	-59.0	38.9	16.1	-4.2	-4.7	19.3	27.8	37.9
I 8	5.4	-1.4	2.1	4.3	6.4	-0.9	-1.1	-15.3	-4.3	42.1
O	28.3	-25.3	-27.6	-29.2	24.8	-25.3	-27.1	-30.7	-30.2	29.4

H: Hidden layer; I1: Input layer 3 - S_{BET} ; I2: Input layer 4 - D_{ave} ; I3: Input layer 5 - V_{por} ; I4: Input layer 6 - V_{mic} ; I5: Input layer 7 - V_{mes}; I6: Input layer 8 - I_D/I_G ; I7: Input layer 9 - R_s ; I8: Input layer 10 - N(%); O: Output layer.

Reference:

1. X. Wei, H. Zou and S. Gao, *Carbon*, 2017, **123**, 471-480.
2. X. Wei, Y. Li and S. Gao, *J. Mater. Chem. A*, 2017, **5**, 181-188.
3. W. C. Long Qie, Henghui Xu, Xiaoqin Xiong,Yan Jiang, Feng Zou,, *Energy & Environmental Science*, 2013, **6**, 2497.